

Dynamical evidence from the sub-parsec counter-rotating disc for a close binary of supermassive black holes in NGC 1068

Jian-Min Wang^{1,2,3}★, Yu-Yang Songsheng^{1,2}, Yan-Rong Li¹, Pu Du¹ and Zhe Yu^{1,2}

¹Key Laboratory for Particle Astrophysics, Institute of High Energy Physics, Chinese Academy of Sciences, 19B Yuquan Road, Beijing 100049, China

²School of Astronomy and Space Sciences, University of Chinese Academy of Sciences, 19A Yuquan Road, Beijing 100049, China

³National Astronomical Observatories of China, Chinese Academy of Sciences, 20A Datun Road, Beijing 100020, China

ABSTRACT

A puzzle in NGC 1068 is how to secularly maintain the counter-rotating disc (CRD) from 0.2 to 7 pc unambiguously detected by recent ALMA observations of molecular gas. Upon further dynamical analysis, we find that the Kelvin-Helmholtz (KH) instability (KHI) results in an unavoidable catastrophe for the disc developed at the interface between the reversely rotating parts. We demonstrate that a close binary of supermassive black holes provides tidal torques to prevent the disc from the KH catastrophe and are led to the conclusion that there is a binary black hole at the center of NGC 1068. The binary is composed of black holes with a separation of 0.1 pc from GRAVITY/VLTI observations, a total mass of $1.3 \times 10^7 M_\odot$ and a mass ratio of ~ 0.3 estimated from the angular momentum budget of the global system. The KHI gives rise to a gap without cold gas at the velocity interface which overlaps with the observed gap of hot and cold dust regions. Releases of kinetic energies from the KHI of the disc are in agreement with observed emissions in radio and γ -rays. Such a binary is shrinking on a timescale much longer than the local Hubble time via gravitational waves, however, the KHI leads to an efficient annihilation of the orbital angular momentum and a speed up merge of the binary, providing a new mechanism for solving the long standing issue of “final parsec problem”. Future observations of GRAVITY⁺/VLTI are expected to be able to spatially resolve the CB-SMBHs suggested in this paper.

Key words: galaxies: active – accretion, accretion discs; black holes: binary

1 INTRODUCTION

For many decades, the Seyfert 2 galaxy NGC 1068 served as an archetype for the unification model of active galactic nuclei (Antonucci 1993) and has received the most intensive observations from radio, infrared, optical, ultraviolet, X-ray and γ -ray bands, which had been individually reported by several hundreds of papers (see Appendixes for some details). It is brighter than 9.1 mag with a redshift of $z = 0.003793$ and a distance of 14.4 Mpc). However, the nature of the NGC 1068 nucleus, obscured by the dusty torus still remains unknown.

ALMA targeted CO (6 – 5) molecular line and resolved a 7 – 10 pc geometrically thick-disc structure in NGC 1068. The dynamics shows non-circular motions and enhanced turbulence superposed on a surprisingly slow rotation pattern of the disc (Garcia-Burillo et al. 2016; Gallimore et al. 2016). However, recent ALMA observations of HCN gas spatially resolved a counter-rotating disc (CRD) from 0.5 – 1.2 pc and beyond reversely extended to 7 pc in the velocity map of HCN gas (Imanishi et al. 2018; Impellizzeri et

al. 2019). In particularly, it has been found that the outer disc shows Keplerian rotation consistent with extrapolation from the inner disc (Impellizzeri et al. 2019), providing invaluable information of the CRD lifetime.

It has been realized that the CRD formation could be related somehow with potential fates of the two streamers at ~ 10 pc scale developed from the south and the north tongues by SINFONI/VLT (Müller Sánchez et al. 2009; Gravity et al. 2020). Random collisions of molecular clouds from large scale distances drive them into nuclear regions and trigger Seyfert activity (Sanders 1981). Two tongues around the central black hole are formed by this way, and later could lead to formation of the CRD in NGC 1068. As to the CRD one must explain how it avoids being destroyed by the KHI on orbital time-scales. Since this directly conflicts with the presence of the observed CRD, the mechanism that is secularly maintaining it at least as long as the viscosity timescale remains a puzzle.

In this paper, we demonstrate that the CRD could be secularly maintained by a close binary of supermassive black holes (CB-SMBHs) supplying angular momentum to the CRD and avoiding the KH catastrophe. A model based on observations is provided for the binary system with a counter-rotating circumnuclear disc. Such

★ E-mail: wangjm@ihep.ac.cn

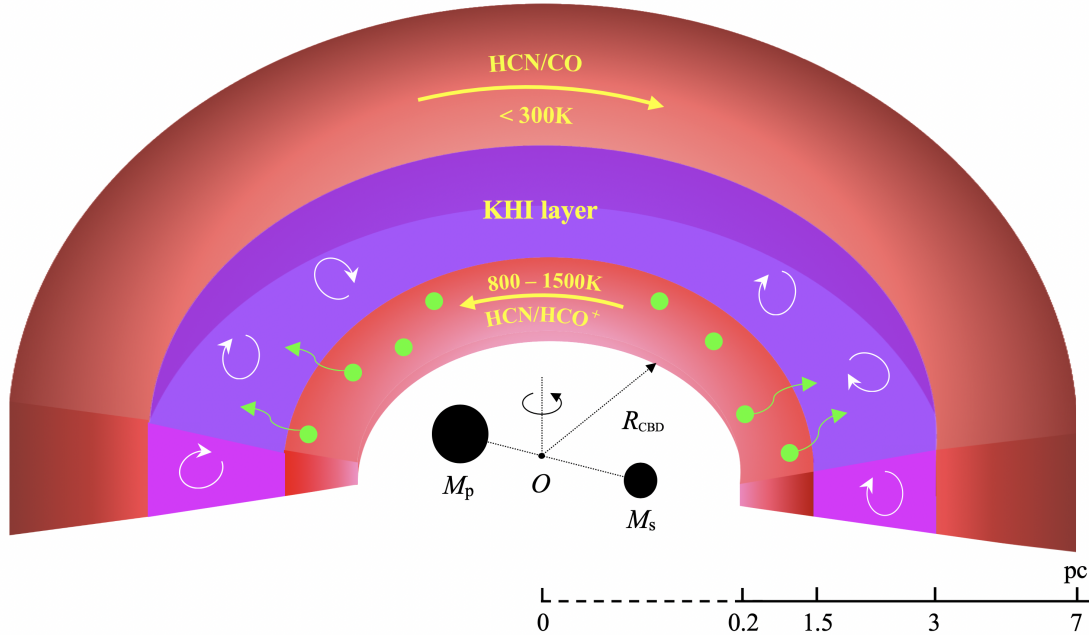


Figure 1. Cartoon of a close binary of supermassive black holes maintaining one circumbinary disc (CBD) composed of the prograde ($R \lesssim 1.5$ pc) and the retrograde ($3 \text{ pc} \lesssim R \lesssim 7$ pc) parts in NGC 1068 observed by ALMA (Impellizzeri et al. 2019) and MIDI/VLTI (Raban et al. 2009). The heights measured by MIDI are $H_0/R \sim 0.3$ (inner part) and ~ 0.6 (outer part), respectively (see details in the text). $R_{\text{CBD}} \sim 0.24$ pc is the inner edge of the CBD measured by GRAVITY (Gravity et al. 2020), which is consistent with dust sublimation radius. The prograde part is the NIR emission regions where water maser clouds (green circles) are co-spaced. The retrograde part is the FIR emission regions. The red color represents the dusty molecular disc (HCN, HCO^+ and CO) radiating in infrared. The interface regions in purple between the prograde and the retrograde parts are undergoing the Kelvin-Helmholtz instability (KHI) to form shocks and turbulences, driving formation of a gap with a width of $\delta R \approx 0.82 M H_0$. The KHI dissipates the kinetic energy of the counter rotating disc giving rise to bremsstrahlung emissions observable in radio with morphology tightly related to the disc shapes. Moreover, shocks in the KHI layer accelerate some electrons to be relativistic to radiate γ -ray emissions observed by *Fermi*-LAT.

a system is showing evidence for an efficient way of removing the angular momentum through the retrograde accretion to harden the binaries.

2 THE CIRCUMNUCLEAR DISC SUPPORTED BY BINARY BLACK HOLES

2.1 Anatomy of the CBD in NGC 1068

Figure 1 shows the geometric structure of the CRD obtained from ALMA, VLTI/MIDI, GRAVITY, VLBI and BLVI (see details in Appendix A). The CRD of HCN molecular gas in NGC 1068 is composed of the inner counterclockwise (prograde: $0.5 - 1.2$ pc) and the outer clockwise rotation (retrograde: < 7 pc) parts distinguished by the interface radius around $R_* \approx 2.5$ pc revealed from the velocity map (Impellizzeri et al. 2019).

The black hole mass has been measured by water maser dynamics (Greenhill et al. 1996, 1997), but corrected for some effects of massive disc gravity (Hure et al. 2002, 2011; Lodato & Bertin 2003). However, mass of the disc within a few parsec is still dominated by the central black hole (Imanishi et al. 2018), questioning the validity of the corrections. Neglecting the uncertainties, we take the black hole mass of $\sim 10^7 M_\odot$ in this paper, which should be robust. On the other hand, NGC 1068 is a prototypical oval galaxy with an unusually massive pseudobulge (Kormendy & Ho 2013) of $M_{\text{bulge}} = 10^{10.9 \pm 0.1} M_\odot$ and stellar dispersion velocity of $\sigma_e = 151 \pm 7 \text{ km s}^{-1}$. Usually, pseudobulges are located below the

well-known $M_\bullet - \sigma$ relation (Tremaine et al. 2002), the upper limits of the black holes are $M_\bullet < 3 \times 10^7 M_\odot$ from this relation.

The KHI driven by shear collisions is unavoidable at interface regions, making the CRD lifetime just comparable with the Keplerian rotation timescale of $t_K = \Omega_K^{-1} = 1.3 \times 10^4 M_7^{-1/2} R_{2\text{pc}}^{3/2}$ yrs through efficient annihilation of angular momentum (AM) simply estimated by the linear analysis (Quach et al. 2015), where $R_{2\text{pc}} = R/2$ pc is the radius of disc and $M_7 = M_\bullet/10^7 M_\odot$ is the black hole mass. This is the KH catastrophe of the CRD in NGC 1068. For a thin disc keeping a vertical equilibrium, it secularly evolves with the viscosity timescale (Pringle 1981, 1991) of $t_{\text{vis}} \approx \alpha^{-1} h^{-2} t_K = 1.3 \times 10^7 \alpha_{0.1}^{-1} h_{0.1}^{-2} M_7^{-1/2} R_{2\text{pc}}^{3/2}$ yrs, where $\alpha = 0.1 \alpha_{0.1}$ is the viscosity parameter, $h = H_0/R = 0.1 h_{0.1}$ is the scale height of the disc. Observations show that the disc of HCN gas follows Keplerian rotations in the both prograde and retrograde parts (Impellizzeri et al. 2019), indicating that the two parts are in dynamical equilibrium and therefore already exist at least as long as a lifetime of t_{vis} .

2.2 Kelvin-Helmholtz instability

The CRD is supersonically rotating. The Mach number of disc rotation is $\mathcal{M} = v_K/c_s^0 \approx (H_0/R)^{-1} = 10 h_{0.1}^{-1}$ from $H_0 = c_s^0/\Omega_K$, where $v_K = R\Omega_K$ is the rotation velocity and c_s^0 is the sound speed outside the KHI layer. In this paper, the subscripts of \oplus and \ominus symbols denote the prograde and retrograde rotations, respectively. In NGC 1068, GRAVITY observations show $h \lesssim 0.14$ in the dust sublimation ring, but $h \approx 0.3$ for the $R \lesssim 1.2$ pc regions (near infrared

regions with temperatures of 800–1500 K), namely, $M_{\oplus} \sim 3$. In the mid-infrared regions ($\gtrsim 3$ pc regions with temperatures $\lesssim 300$ K) (Raban et al. 2009), we have $h \approx 0.6$, as a geometrically slim, and $M_{\oplus} \approx 1.7$. Being different from the well-understood normal KHI modes (Drazin 2002), both the prograde and the retrograde parts as supersonic flows lead to an extremely complicated interface from AM cancellations subject to black hole gravity and fast cooling of the hot plasma heated by the formed shocks. We take the simplest approach using the Rankine-Hugoniot conditions of shocks for the supersonic collisions of two streams in a slab geometry (Lee et al. 1996). Both the prograde ($v_1 = v_K$) and retrograde ($v_2 = -v_1$) parts have the same Keplerian velocity (v_K) but they have densities of ρ_0 and $\chi\rho_0$ ($\chi \leq 1$) at the interface, respectively, where χ is the density ratio depending on properties of the CRD. The velocity, density and pressures of the post shock regions are $v/v_K = (1 - \sqrt{\chi})/(1 + \sqrt{\chi})$, $\rho/\rho_0 = (\Gamma + 1)/(\Gamma - 1)$ and $p = 2(1 + \Gamma)\chi(1 + \sqrt{\chi})^{-1}\rho_0 v_K^2$, respectively, where Γ is the adiabatic index. For the case with identical densities ($\chi = 1$), we have the most efficient dissipation of the kinetic energy into the thermal since $v = 0$. This gives rise to multiwavelength emissions tightly related to the dynamical structure of this region.

Supposing the interface radius (R_{KHI}) with a thickness of δR , the AM cancellation driven by the KHI is happening with a timescale of $t_{\text{KHI}} \approx \Omega_K^{-1}$ and $\delta R \approx t_{\text{KHI}} v_R$, where v_R is the velocity of gas entering the KHI zone. In a linear analysis, V_R is given by the viscosity stress, which is much smaller than the sound speed (c_s) in the KHI layer formed due to shear collisions. In the present context, however, we have $v_R \approx c_s$ in the layer because the efficient dissipation of the kinematic energy of the interface layer heats the medium and the waves propagate with c_s . With the shock conditions, we have $c_s^2 = p/\rho = 2\chi(1 + \sqrt{\chi})^{-1}(\Gamma - 1)v_K^2 = (2/3)v_K^2$, for $\chi = 1$ and $\Gamma = 5/3$, which results in the KHI gas to have two thirds of the virial temperatures. Considering $H_0 = c_s^0 \Omega_K^{-1}$, we have the layer width approximated by $\delta R \approx t_{\text{KHI}} c_s \approx 0.82 \Omega_K^{-1} v_K = 0.82 M H_0$. For the current case of NGC 1068, the interface of the density map is not resolved by the current ALMA observations (Impellizzeri et al. 2019), but the velocity interface is quite clear from the velocity map (see Figure 2 in Impellizzeri et al. (2019)). The projected radius is about $R_* \approx 2.5$ pc, which exactly overlaps with the geometrical gap between the NIR and MIR component (Raban et al. 2009). We thus take the interface radius $R_{\text{KHI}} = R_*$. For the simplest estimation, we just take $M_{\text{KHI}} \approx 2.5$ before shear collisions, which is the averaged value between the NIR and MIR regions. The KHI layer therefore has a width of $\delta R \approx 2 H_0 \approx 1.6$ pc, where $H_0 \approx 0.8$ pc is the averaged height of the NIR and MIR regions in light of observations (Raban et al. 2009). This gap should be observed in density map, however, it is not spatially resolved (1.4 pc for NGC 1068) of the current ALMA (Impellizzeri et al. 2019). However, we note that the width of the gap is affected by the prograde part supported by the tidal torques of one CB-SMBH.

The KH catastrophe can be evaluated by AM distributions of the CRD. The total AM of the retrograde part (within 7 pc) can be estimated by $\mathcal{J}_{\ominus} \approx -M_{\text{gas}}^{\oplus} v_K \bar{R}_{\ominus} \approx -325.3 M_7^{1/2} M_{\odot} \text{pc}^2 \text{yr}^{-1}$, where $\bar{R}_{\ominus} = 5$ pc is the averaged radius of the retrograde regions (3–7 pc), and $v_K \approx 10^7 \text{ cm s}^{-1}$ at this radius. For the prograde part (< 1.5 pc), we have the total AM of $\mathcal{J}_{\oplus} \approx 190.9 M_7^{1/2} M_{\odot} \text{pc}^2 \text{yr}^{-1}$, where we take $M_{\text{gas}}^{\oplus} = 9 \times 10^5 M_{\odot}$ and the averaged radius $\bar{R}_{\oplus} = 1$ pc. Owing to $|\mathcal{J}_{\oplus}| < |\mathcal{J}_{\ominus}|$, the prograde part will be destroyed by the retrograde via the KHI action. Given an AM distribution of a disc as $\mathcal{J} \propto R^{\beta}$ ($\beta > 0$), the cancelled AM can be estimated by $\delta\mathcal{J}/\mathcal{J} = \beta(\delta R/R_{\text{KHI}})$. From $\delta R \approx 0.82 M H_0$,

we have $\delta\mathcal{J}/\mathcal{J} \approx 0.82\beta$. Though the gaseous dynamics has been measured in NGC 1068, the spatial distribution of mass density is poorly done. In the 14 pc \times 10 pc regions (Imanishi et al. 2018), the mass is about $2 \times 10^6 M_{\odot}$ corresponding to an averaged surface density of $\Sigma_{\text{gas}}^{\oplus} \approx 1.4 \times 10^4 M_{\odot} \text{pc}^{-2}$ over this region. We have $\Sigma_{\text{gas}} \propto R^{-0.6}$ from the prograde ($\bar{R}_{\oplus}, \Sigma_{\oplus}$ given in SM) to retrograde ($\bar{R}_{\ominus}, \Sigma_{\ominus}$) parts, giving rise to $\mathcal{J} \propto R^{1.9}$. With $\beta \approx 1.9$, we find that the AM of the CRD can be cancelled completely by once action of the KHI within a dynamical timescale of $t_{\text{KHI}} \sim \Omega_K^{-1} = 1.9 \times 10^4 M_7^{-1/2} (R_{\text{KHI}}/R_*)^{3/2} \text{ yrs}$. This is a very short timescale compared with the typical AGN lifetime, even the flickering lifetime ($\sim 10^5 \text{ yrs}$) (Schawinski et al. 2015). It would be worse for the prograde part if the retrograde part is able to obtain more AM from the outer boundary. The KH catastrophe cannot be avoided unless there is an extra supplement from external sources of torque. Obviously, the only way to maintain the prograde part is the gain AM from a CB-SMBH.

2.3 Close binary of supermassive black holes

As seen in a brief review in Appendix B, evidence for a CB-SMBH is still quite elusive in observations though there are a few candidates. Starting from one CB-SMBH with a circular orbit of a separation (A) composed of the primary (M_p) and the secondary (M_s), we have its period of $P_{\text{orb}} \approx 877(1 + q)^{-1/2} M_7 a_5^{3/2} \text{ yrs}$, and orbital AM of $\mathcal{J}_B = 656.2 q(1 + q)^{-1/2} M_7^2 a_5^{1/2} M_{\odot} \text{pc}^2 \text{yr}^{-1}$, where $q = M_s/M_p$ is the mass ratio, $a = A/R_{\text{Sch}}$, $a_5 = a/10^5$, $R_{\text{Sch}} = 2GM_p/c^2 = 3.0 \times 10^{12} M_7 \text{ cm}$ is the Schwarzschild radius, G is the gravitational constant and c is the speed of light. The tidal torques of one CB-SMBH strongly interact with its circumbinary disc (CBD) to form a cavity with an inner radius of $R_{\text{CBD}} = 2A$ in light of analytical calculations and simulations (Artymowicz et al. 1994; Armitage et al. 2002). In Appendix C, we demonstrate that $2\mu\text{m}$ -imaged hole discovered by GRAVITY (Gravity et al. 2020) is approximate to $R_{\text{CBD}} = 0.24$ pc with help of the gas dynamics of ALMA-detected CRD. The timescale of gravitational waves is given by $t_{\text{GW}} = 2.0 \times 10^{14} M_7 a_5^4 / q(1 + q) \text{ yrs}$ for circular orbits (Peters 1964) much longer than the Hubble time, which is the well-known “final parsec problem”. To maintain the prograde part, we need $\mathcal{J}_B \gtrsim \mathcal{J}_{\oplus}$, yielding $q \gtrsim 0.3$ (for $M_7 = a_5 = 1$) in order to make up for the AM loss due to the KHI action.

The CBD regions governed by the tidal torques of the CB-SMBH can be estimated in a simple way. Tidal forces can be approximated by $F_{\text{tid}} \approx (GM_{\text{tot}} \delta m / R^2) (A/R)$ for a point mass of δm , which is about perpendicular to the direction to the center, and the corresponding torques are $\mathcal{T}_{\text{tid}} \approx F_{\text{tid}} R = \delta m(1 + q)c^2 a r^{-2} / 4$, where $r = R/R_{\text{Sch}}$. Taking the ratio of the gas parcels angular momentum ($\Delta\mathcal{J}$) and the binary torque ($\Delta\mathcal{T}_{\text{tid}}$), we define the tidal timescale of $t_{\text{tid}} = \Delta\mathcal{J}/\mathcal{T}_{\text{tid}}$, where $\Delta\mathcal{J} = \delta m(1 + q)^{1/2} R_{\text{Sch}} c r^{1/2} / \sqrt{2}$, yielding $t_{\text{tid}} = (1 + q)^{-1/2} (a/r)^{-1} t_K$. Considering the rapid decays of the tidal torques with radius (Papaloizou & Lin 1984; Pringle 1991), we recast the tidal timescales of $t_{\text{tid}} = \varepsilon_0(1 + q)^{-1/2} (a/r)^{-4} t_K$, where $\varepsilon_0 \approx 0.1$. In the tidal-governed regions $t_{\text{tid}} \leq t_{\text{vis}}$, we have the critical radius of $R_{\text{tid}} \leq 10 (\varepsilon_{0.1} \alpha_{0.1})^{-1/4} h_{0.1}^{-1/2} (1 + q)^{1/8} A$, where $\varepsilon_{0.1} = \varepsilon_0/0.1$, beyond which the viscosity torques becomes dominant. For NGC 1068, we have $R_{\text{tid}} \approx 1.2$ pc for typical values ($\varepsilon_{0.1}, \alpha_{0.1}, h_{0.1}$) = 1, which is in agreement with the sizes of the prograde part (Impellizzeri et al. 2019). Such a CB-SMBH guarantees the stability of the prograde part and prevents it from the KH catastrophe.

The gas disc beyond R_{tid} is jointly governed by viscosity stress and the tidal torques, and its outer boundary conditions. Since $R > R_{\text{tid}}$ part is retrograde with respect to the CB-SMBH orbits, it loses AM due to the tidal torques, enhancing accretion onto the center (Nixon et al. 2011; Roedig & Sesana 2014; Bankert et al. 2015). In the context of the inner part as a decretion disc (Pringle 1991), its outer boundary moves outward with the viscosity timescale but encounters the inward flows from the retrograde part, leading to an equilibrium radius (R_{KHI}) between the inward and the outward flows. Dynamical evolution of the CRD could compress the width of the gap. Numerical simulations are expected for details of such a complicated case. For NGC 1068, $\mathcal{J}_B > |\mathcal{J}_\oplus + \mathcal{J}_\ominus|$ indicates that the CB-SMBH with a total mass of $1.3 \times 10^7 M_\odot$, mass ratio of $q = 0.3$ and a separation of 0.1 pc can support this observed CRD in the galactic center.

On the other hand, the CB-SMBH in NGC 1068, as the first observed object, faces the well-known “final parsec problem” (Begelman et al. 1980; Goicovic et al. 2018). With the orbital parameters obtained presently, we can estimate the orbital evolution purely driven by gravitational waves. According to Peters (1964), the shrinking timescale of orbits is given by $t_{\text{GW}} = 1.24 \times 10^{13} a_5^4 M_7 / q(1+q)$ yrs, which is much longer than the Hubble time and episodic lifetime of AGNs. This indicates that the CB-SMBHs can not merger via radiations of GWs within the Hubble time, showing “the final parsec problem”. Successive series of random accretion of molecular clouds onto binary black holes have been suggested by simulations (Goicovic et al. 2018), fortunately, from observational side, two tongues from south and north direction around the center appear in NGC 1068 ~ 10 pc regions (Müller Sánchez et al. 2009). The retrograde part can efficiently cancel the binary orbital AM through the KHI of random and episodic accretion. The episodic numbers can be roughly estimated by $N = \mathcal{J}_B / |\mathcal{J}_\oplus + \mathcal{J}_\ominus|$, and accretion with low AM (i.e., $|\mathcal{J}_\oplus + \mathcal{J}_\ominus| \approx 0$) can efficiently shrink the CB-SMBH in light of $t_{\text{GW}} \propto M_p^{-3}$ for the case given A. For NGC 1068, we have $N \approx 4.8$ from ALMA observations (Imanishi et al. 2018; Impellizzeri et al. 2019). This indicates that the retrograde accretion onto CB-SMBHs is an efficient way of removing orbital AM of the binaries.

2.4 Multi- λ emissions

During the AM cancellation through the KHI, a huge amount of kinematic energies of the CRD is released, which can be estimated by $\Delta E_K \approx \Delta M_{\text{KHI}} v_K^2$ within the interval of Ω_K^{-1} . The radiative luminosity from the dissipation is given by $L_{\text{KHI}} \approx (\Delta M_{\text{KHI}} / \Delta t_{\text{KHI}}) v_K^2 = \ell_* \dot{M}_{\text{torus}} c^2$, where $\ell_* = 1/(r_* r_{\text{KHI}} \alpha h^2) = 2 \times 10^{-4} \alpha_{0.1}^{-1} h_{0.1}^{-2}$ (taking $r_{\text{KHI}} = 1$ and $r_* = R_*/R_{\text{Sch}} = 5 \times 10^6$) and \dot{M}_{torus} is the accretion rates of the torus. For the typical values of the parameters, we have $L_{\text{KHI}} \approx 1.1 \times 10^{44} \dot{M}_1 \text{ ergs s}^{-1}$ at the peak frequency of $\epsilon_{\text{peak}} \sim 0.1 r_{\text{KHI}}^{-1} \text{ keV}$ from the hot KHI layer during the interval of the KHI timescale, where $\dot{M}_1 = \dot{M}_{\text{torus}} / 10 M_\odot \text{ yr}^{-1}$. The infall with a typical rate of $10 M_\odot \text{ yr}^{-1}$ at a few parsec scales in NGC 1068 has been observed by SINFONI (Müller Sánchez et al. 2009; García-Burillo et al. 2019) (most of this rate will be channeled into outflows). Such a powerful emission can be detectable in type 1 AGNs, however, for NGC 1068 as a Compton thick AGN (Zaino et al. 2020), the major emissions from the KHI layer will be undetectable because of absorption of the torus along the line of sight. The KHI provides a new explanation of soft X-ray excess if there is a CRD like in NGC 1068. The excess should be relatively stationary because of its origins from a large scale.

On the other hand, fortunately, radio emission from this HKI dissipation is detectable, which can be estimated by the bremsstrahlung emission from the KHI layer. The shear collisions of the two streamers make the post-shocked gas with temperatures close to the virial one as $T_{\text{gas}} \approx 1.2 \times 10^6 r_{\text{KHI}}^{-1} \text{ K}$, where $r_{\text{KHI}} = R_{\text{KHI}}/R_*$. Since the bremsstrahlung cooling timescale of hot plasma is (Rybicki & Lightman 1979) $t_{\text{cool}} \approx 3.0 n_6^{-1} T_6^{1/2} \text{ yrs}$, the KHI layer can be efficiently cooled, where $n_6 = n_e / 10^6 \text{ cm}^{-3}$ is the density (about the CRD gas density) and $T_6 = T / 10^6 \text{ K}$ is the layer temperature. The fast cooling ($t_{\text{cool}} \ll \Omega_K^{-1}$) prevents the shocks from propagation outside the layer. Owing to the black hole gravity, the cooled layer will rapidly collapse onto the prograde part with the free-fall timescale of $t_{\text{ff}} \approx 1.8 \times 10^4 r_{\text{KHI}}^{3/2} \text{ yrs}$. On the other hand, gas is supplied beyond the KHI layer with a timescale of $t_{\text{vis}} \approx 10^3 \alpha_{0.1}^{-1} h_{0.1}^{-2} t_K$ by the viscous stress from the retrograde part. The comparison of $t_{\text{cool}} \ll t_{\text{KHI}} \sim t_{\text{ff}} \ll t_{\text{vis}}$ implies that the gas supply to the layer will be halted. The cooled gas in the layer will be emptied by the gravity of the central black holes, forming a gap with a width of δR . Fortunately, such a gap has been revealed by MIDI/VLTI, showing spatial separations between the NIR (hot dust with temperature $> 800 \text{ K}$, and located $< 1.4 \text{ pc}$) and MIR ($< 300 \text{ K}$, and located $> 3 \text{ pc}$) emissions (Raban et al. 2009).

With the KHI layer’s volume of $V_{\text{KHI}} = 2\pi R_{\text{KHI}} \delta R H_0 = 1.6\pi R_{\text{KHI}}^3 \mathcal{M} (H_0/R)^2$, we have radio emissions of $L_{256\text{GHz}} = 1.0 \times 10^{39} n_6^2 T_6^{-1/2} R_{2.5}^3 h_{0.1}^2 \text{ ergs s}^{-1}$ at $\nu = 256 \text{ GHz}$ according to the thermal emissivity [Eq. 5.14b in Rybicki & Lightman (1979)]. This radio emission agrees with 12.7 mJy observed by ALMA (Impellizzeri et al. 2019) at 256 GHz. As emitted from the layer, the radio morphology should follow the velocity interface. Indeed, this agrees with the observations by comparing the radio 256 GHz map with the HCN velocity map from Figure 2 in Impellizzeri et al. (2019), showing the north-east part of the HCN disc and southwest part where the velocity interfaces matches the radio morphology. Moreover, the layer has a luminosity of $L_{5\text{GHz}} \approx 2.0 \times 10^{37} \text{ ergs s}^{-1}$ at 5 GHz from bremsstrahlung emissions, which roughly agrees with the compact radio source S_1 in the nuclear center.

Additionally, the strong shocks unavoidably accelerate some electrons to be relativistic in the KHI layer, leading to non-thermal high energy emissions from the layer. Fermi-LAT observations (Ajello et al. 2017) detected a γ -ray luminosity of about $2.5 \times 10^{41} \text{ ergs s}^{-1}$ with a cut-off energy of $\sim 10^2 \text{ GeV}$ detected by MAGIC (Acciari et al. 2019). Jet model and starburst model are suggested, but origins of the GeV emissions remain open (Acciari et al. 2019) [starburst model is not able to produce the observed GeV emissions, see Figure 2 in Acciari et al. (2019)]. Here the dissipation of the KHI layer could provide an alternative explanation. Magnetic fields are of $B = 10^{-3} \text{ Gauss}$ in this region (Krolik & Begelman 1987). The shock velocity is $V_{\text{sh}} \sim 3 \times 10^7 T_6^{1/2} \text{ cm s}^{-1}$, if $\Gamma = 5/3$, yielding the acceleration timescale of $t_{\text{acc}} = R_L c / V_{\text{sh}}^2 = 5.8 \times 10^6 \gamma_5 B_{-3}^{-1} T_6 \text{ sec}$, where $\gamma_5 = \gamma / 10^5$ is the Lorentz factor of relativistic electrons, R_L is the Lamore gyration radius (Blandford & Eichler 1987). The energy density of infrared photons is about $U_{\text{IR}} = 1.8 \times 10^{-6} L_{43} R_{\text{pc}}^{-2} \text{ ergs cm}^{-3}$ dominating over the magnetic fields, where $L_{43} = L_{\text{IR}} / 10^{43} \text{ ergs s}^{-1}$ is the infrared luminosity and $R_{\text{pc}} = R / 1 \text{ pc}$ is the distance of the accelerating regions to the center. In such a context, the cooling of the electrons is governed by inverse Compton scatter and given by $t_{\text{IC}} = 3m_e c / 4\sigma_T \gamma U_{\text{IR}} = 1.7 \times 10^8 \gamma_5^{-1} L_{43}^{-1} R_{\text{pc}}^2 \text{ sec}$ (Rybicki & Lightman 1979), and the relativistic electrons contribute less in radio band. The maximum Lorentz factor is $\gamma_{\text{max}} =$

$5.5 \times 10^5 L_{43}^{-1/2} R_{\text{pc}} B_{-3}^{1/2} T_6^{-1/2}$ from $t_{\text{IC}} = t_{\text{acc}}$. The maximum energetic photons are $\epsilon_{\text{max}} \approx \gamma_{\text{max}}^2 \epsilon_{\text{IR}} = 74 (\gamma_{\text{max}}/\gamma_0)^2 \epsilon_{0.25}$ GeV, where $\gamma_0 = 5.5 \times 10^5$, $\epsilon_{0.25} = \epsilon_{\text{IR}}/0.25$ eV is IR photon energy in units of $\lambda = 5 \mu\text{m}$ estimated from the spectral energy distribution (Gravity et al. 2020). If the total budget of γ -rays is conservatively 1% [see Blandford & Eichler (1987)] of L_{KHI} , about $10^{42} \text{ ergs s}^{-1}$ is produced that is enough to explain the observed γ -rays.

3 DISCUSSIONS

3.1 Magnetic fields

We first consider the role of a strong azimuthal magnetic field to support the CRD. The Alfvén velocity is given by $v_A = B_\phi / \sqrt{\mu_0 \rho_0}$, where B_ϕ is the azimuthal component of the magnetic field, μ_0 is permeability of free space and ρ_0 is the density of gas. The plasma couples with neutral part tightly so that the magnetic fields controlling plasma govern the neutral part of gas. If the azimuthal magnetic field supports the CRD, the Alfvén waves provide enough energy to secularly support the CRD, namely $v_A^2 \geq (t_{\text{vis}}/t_K) (\Delta V)^2$, where $\Delta V \approx 2v_K$ is the differential velocity of the CRD. The magnetic field is given by

$$B_\phi \geq 662 \alpha_{0.1}^{-1/2} h_{0.1}^{-1} \rho_{-18}^{1/2} v_2 \text{ mG}, \quad (1)$$

where $\rho_{-18} = \rho_0/10^{-18} \text{ g cm}^{-3}$ [the ALMA-observed density of gas from the HCN line (Imanishi et al. 2018)] and $v_2 = v_K/10^2 \text{ km s}^{-1}$. Recent polarization observations show $B \approx 0.7 \text{ mG}$ in the few parsec regions of its circumnuclear region (Lopez-Rodriguez et al. 2020) in NGC 1068, which is much lower than the lower limit of the magnetic fields to support the CRD. This directly rules out the magnetic fields to support the unusual CRD.

3.2 A CRD around a single SMBH

Since nuclear regions are much smaller than the circumnuclear disk, random accretion onto black holes is naturally taking place (Sanders 1981; King & Pringle 2006). In a cosmic timescale, such a kind of the random accretion leads to spin-down evolution of SMBHs as a result of cancellations of spin AM from different episodes (Kuznetsov et al. 1999; King et al. 2008), but speeds up cosmic growth of SMBHs due to low radiation efficiency. According to the cosmic evolution of duty cycle of SMBH activity episodes (Wang et al. 2006), the spin-down behaviors of SMBH evolution are found from application of cosmic equation of radiative efficiency to the survey data (Wang et al. 2009; Li et al. 2012), providing strong evidence for the random accretion. In particular, cold clumps are universal in galaxies (Tremblay et al. 2016; Temi et al. 2018). On the other hand, this indicates that there were a series of CRDs across cosmic time. The CRD will give rise to very fast accretion onto SMBHs [also see Ref (Kuznetsov et al. 1999; Quach et al. 2015; Dyda et al. 2015)] and show some imprints at scale of a few parsec. Is there any independent evidence for this?

Thanks are given to recent ALMA observations of nearby Seyfert galaxies for a new clue to understanding this issue. Among this sample, three Seyfert galaxies (NGC 1365, NGC 1566 and NGC 1672) show a gas hole or depletion in the center within a few parsec (Combes et al. 2019), of which two are more nearby than NGC 1068. It is very interesting to note that NGC 1365 and NGC 1566 are changing-look AGNs. NGC 1365 is changing its column density from Compton-thick to -thin (Winter et al. 2009) whereas NGC 1566 is changing spectral type (Oknyansky et al.

2019). We preliminarily speculate that the gas hole could be caused by the KHI, which leads to AM annihilation of CRDs depleting the parsec scale regions. If this happened, a fast collapse onto very central regions results in high accretion rates of AGNs. The parsec scale hole of gas could be an indicator of the remnant of a past CRD around a single SMBH. Considering the short lifetime of a CRD around single SMBH as low as $t_{\text{KHI}}/t_{\text{vis}} \sim 10^{-3}$, we think that the CRD will be detected in an extremely low opportunity. Future MUSE observations of ALMA-observed targets should explore detailed structure at a few parsec scales to test if there are something related to “two tongues” in NGC 1068 (Müller Sánchez et al. 2009). Additionally, we should check their polarized spectra for optical Fe II emission lines for accretion status of the central black holes (Du & Wang 2019). On the other hand, candidate AGNs harboring CB-SMBHs with CRDs can be selected from Seyfert 2 galaxies whose polarized spectra show asymmetric profiles of broad emission lines.

3.3 Disc geometry

For simplicity, we apply the Rankine-Hugoniot calculation to the slab geometry of the CRD in this paper, allowing us to focus on analysis of the major effects of the KHI action and tidal interaction of the CB-SMBHs with its circumbinary disk in a simple way. Following Quach et al. (2015) and Dyda et al. (2015), we will make use of disc geometry of the counter-rotating gas for detailed analysis of the KHI and its effects in the future. The violent dissipation of the kinetic energies of the counter-rotating motion gives rise to gas expansion in the vertical direction so that we have to study 3-dimensional processes, such as outflows from the disc surface, which could be probably related with the observed in this region. All these are beyond the scope of this paper, but we will carry out detailed applications of the KHI theory to NGC 1068 in an separate paper.

4 CONCLUSIONS AND REMARKS

The puzzle of a counter-rotating disc from 0.2 – 7 parsec regions discovered by ALMA observations arises a serious issue how to secularly maintain it. The Kelvin-Helmholtz instability will destroy the disc unless there is an extra supply of angular momentum. A close binary of supermassive black holes is expected to support the unusual disc for a viscosity timescale. The binary black holes are of a total mass of $1.3 \times 10^7 M_\odot$ and mass ratio of $\gtrsim 0.3$ and a separation of 0.1 parsec. With annihilation of angular momentum due to the KHI, the disc efficiently dissipates its kinematic energy into radiation peaking at soft X-rays and radio bands from bremsstrahlung emissions. Though soft X-rays are absorbed by the torus, the radio emissions are in agreement with observations. We also find significant γ -rays from the shocks developed from the KHI, which agrees with *Fermi* and *MAGIC* observations.

The polarized spectra of NGC 1068 show asymmetric profiles of broad H β (with polarization degree of $\sim 3\%$) (Miller et al. 1991) indicating complicated structure of the broad-line regions. In the NIR, the core has a $m_K \approx 8.7 \text{ mag}$ (Gravity et al. 2020), the polarized magnitudes could be of $\sim 12.5 \text{ mag}$ in K-band. The polarized fluxes of broad Brackett line (Martins et al. 2010) could be too weak to detect through the GRAVITY/VLTI. Fortunately, it is strong enough for GRAVITY+ as the next generation of GRAVITY/VLTI to make efforts to spatially resolve the < 0.1 parsec regions for

the appearance of the CB-SMBHs through differential phase curves (Songsheng et al. 2019).

Given the black hole mass, mass ratio and separations, the CB-SMBH is radiating gravitational waves (GW) with frequencies of $f_{\text{GW}} = 0.1 (1 + q)^{1/2} M_7^{-1} a_5^{-3/2}$ nHz and intrinsic strain of amplitudes is $h_s = 5 \times 10^{-19} q M_7 a_5^{-1} d_{14.4}^{-1}$, where $d_{14.4} = d/14.4$ Mpc is the distance of NGC 1068 to observers. GW background composed of NGC 1068-like AGNs can be detected by Square Kilometer Array (SKA) (Barack et al. 2018). However, the retrograde part eventually shrink the CB-SMBH through cancelling its orbital AM to merge, providing a paradigm of solving the “final parsec problem”, which is related with many concomitant phenomenon risen from the KHI. The CB-SMBH in NGC 1068, as one of long-sought-after candidates, has an angular size of 2 mas, which is larger by a factor of 100 than the spatial resolution of the Event Horizon Telescopes (EHT), and is thus worth observing via EHT.

ACKNOWLEDGEMENTS

The authors are grateful to S. Dyda as the referee for a helpful report improving the manuscript. Yao Chen is acknowledged for helpful discussions. Bo-Wei Jiang is thanked for the plot in this paper. JMW acknowledges financial support from the National Science Foundation of China (11833008 and 11991054), from the National Key R&D Program of China (2016YFA0400701), from the Key Research Program of Frontier Sciences of the Chinese Academy of Sciences (CAS; QYZDJ-SSW-SLH007), and from the CAS Key Research Program (KJZD-EW-M06).

REFERENCES

- Acciari, V. A., et al., 2019, *ApJ*, 883, 135
 Ajello, M. et al., 2017, *ApJS*, 232, 18
 Alonso-Herrero, A., Pereira-Santaella, M., García-Burillo, S., et al., 2018, *ApJ*, 859, 144
 Antonucci, R., 1993, *ARA&A*, 31, 473
 Antonucci, R. R., & Miller, J. S., 1985, *ApJ*, 297, 621
 Armitage, P. J., & Natarajan, P., 2002, *ApJ*, 567, L9
 Artymowicz, P., & Lubow, S. H., 1994, *ApJ*, 421, 651
 Bankert, J., Krolik, J. H., & Shi, J., 2015, *ApJ*, 801, 114
 Barack, L., Cardoso, V., Nissanke, S., et al., 2019, *Class. Quant. Grav.*, 36, 143001
 Begelman, M. C., Blandford, R. D. & Rees, M. J., 1980, *Nature*, 287, 307
 Blandford, R., & Eichler, D., 1987, *Phys. Rep.*, 154, 1
 Bowen, D. B., Mewes, V., Noble, S. C., et al., 2019, *ApJ*, 879, 76
 Combes, F., García-Burillo, S., Audibert, A., et al., 2019, *A&A*, 623, A79
 Comerford, J. M., Schluns, K., Greene, J. E., et al., 2013, *ApJ*, 777, 64
 Cuadra, J., Armitage, P. J., Alexander, R. D., & Begelman, M. C., 2009, *MNRAS*, 393, 1423
 Darzin, P. G., Introduction to Hydrodynamic Instability, Cambridge University Press (2002)
 Doan, A., Eracleous, M., Runnoe, J. C., et al., 2020, *MNRAS*, 491, 1104
 D’Orazio, D. J., Haiman, Z., & Schiminovich, D., 2015, *Nature*, 525, 351
 Dotti, M., Sesana, A., & Decarli, A., 2012, *Adv. Astron.*, 2012, 3
 Du, P., Brotherton, M., Wang, K., et al., 2018, *ApJ*, 869, 142
 Du, P., Wang, J.-M., & Zhang, Z.-X., 2017, *ApJL*, 840, L6
 Du, P., & Wang, J.-M., 2019, *ApJ*, 886, 42
 Dyda, S., Lovelace, R. V. E., Ustyugova, G. V., et al., 2015, *MNRAS*, 446, 613
 Ebisuzaki, T., Makino, J., & Okumura, S. K., 1991, *Nature*, 354, 212
 Escala, A., Larson, R. B., Coppi, P. S., et al., 2005, *ApJ*, 630, 152
 Farris, B. D., Duffell, P., MacFadyen, A. I., et al., 2014, *ApJ*, 783, 134
 Fu, H., Myers, A. D., Djorgovski, S. G., et al., 2015, *ApJ*, 799, 72
 Gallimore, J. F., Baum, S. A., O’Dea, C. P., et al., 1996, *ApJ*, 462, 740
 Gallimore, J. F., Baum, S. A., O’Dea, C. P., et al., 1996, *ApJ*, 458, 136
 Gallimore, J. F., Baum, S. A., O’Dea, C. P., et al., 1996, *ApJ*, 462, 740
 Gallimore, J. F., et al., 2004, *ApJ*, 613, 794
 Gallimore, J. F., Elitzur, M., Maiolino, R., et al., 2016, *ApJL*, 829, L7
 Gallimore, J. F., Henkel, C., Baum, S. A., et al., 2001, *ApJ*, 556, 694
 García-Burillo, S., et al., 2019, *A&A*, 632, A61
 García-Burillo, S., Combes, F., Ramos Almeida, C., et al., 2016, *ApJ*, 823, L12
 Gaskell, C. M., 2010, *Nature*, 463, E1
 Gaspari, M., Ruszkowski, M., & Oh, S. P., 2013, *MNRAS*, 432, 3401
 Goicovic, F. G., et al., 2017, *MNRAS*, 472, 514
 Goicovic, F. G., et al., 2018, *MNRAS*, 479, 3438
 Graham, M. J., Djorgovski, S. G., Stern, D., et al., 2015, *MNRAS*, 453, 1562
 Graham, M. J., Djorgovski, S. G., Stern, D., et al., 2015, *Nature*, 518, 74
 Gravity Collaboration, et al., 2020, *A&A*, 634, 1
 Greenhill, L. J., Gwinn, C. R., Antonucci, R., et al., 1996, *ApJL*, 472, L21
 Greenhill, L. J., & Gwinn, C. R., 1997, *Astrophys. Space Sci.*, 248, 261
 Gültekin, K., & Miller, J. M., 2012, *ApJ*, 761, 90
 Huré, J.-M., et al., 2002, *A&A*, 395, L21
 Huré, J. M., Hersant, F., F., Surville, C., et al., 2011, *A&A*, 530, A145
 Imanishi, M., et al., 2018, *ApJL*, 853, L251
 Imanishi, M., Nakanishi, K., & Izumi, T., 2016, *AJ*, 152, 218
 Impellizzeri, C. M. V., et al., 2019, *ApJL*, 884, L28
 Jaffe, W., Meisenheimer, K., Röttgering, H. J. A., et al., 2004, *Nature*, 429, 47
 Kennicutt, R. C., Jr., 1998, *ARA&A*, 36, 189
 Kharb, P., Lal, D. V., & Merritt, D., 2017, *Nat. Astron.*, 1, 727
 King, A. R., & Pringle, J. E., 2006, *MNRAS*, 373, L90
 King, A. R., Pringle, J. E., & Hofmann, J. A., 2008, *MNRAS*, 385, 1621
 Kormendy, J., & Ho, L. C., 2013, *ARA&A*, 51, 511
 Kovacčević, A. B., Wang, J.-M., & Popović, L. C., 2020, *A&A*, 635, A1
 Krolik, J. H., & Begelman, M. C., 1987, *ApJ*, 329, 701
 Kuznetsov, O. A., Lovelace, R. V. E., & Romanova, M. M., 1999, *ApJ*, 514, 691
 Laor, A., & Netzer, H., 1989, *MNRAS*, 238, 897
 Lee, H. M., Kang, H., & Ryu, D., 1996, *ApJ*, 464, 131
 Leighly, K. M., Terndrup, D. M., Gallagher, S. C., et al., 2016, *ApJ*, 829, 4
 Li, Y.-R., Wang, J.-M., Ho, L. C., et al., 2016, *ApJ*, 822, 4
 Li, Y.-R., Wang, J.-M., & Ho, L. C., 2012, *ApJ*, 749, 11
 Li, Y.-R., Wang, J.-M., Zhang, Z.-X., et al., 2019, *ApJS*, 241, 33
 Liu, X., Lazio, T. J. W., Shen, Y., et al., 2018, *ApJ*, 854, 169
 Lodato, G., & Bertin, G., 2003, *A&A*, 398, 517
 Lodato, G., Nayakshin, S., King, A. R., & Pringle, J. E., 2009, *MNRAS*, 398, 1392
 López-Gonzaga, N., Jaffe, W., Burtscher, L., et al., 2014, *A&A*, 565, A71
 Lopez-Rodriguez, E., Alonso-Herrero, A., García-Burillo, S., et al., 2020, *ApJ*, arXiv:1905.08802
 Lopez-Rodriguez, E., Fuller, L., Alonso-Herrero, A., et al., 2018, *ApJ*, 595, 99
 Lopez-Rodriguez, E., Packham, C., Young, S., et al., 2015, *MNRAS*, 431, 2723
 Lutz, D., Genzel, R., Sturm, E., et al., 2000, *ApJ*, 530, 733
 MacFadyen, A. I., & Milosavljević, M., 2008, *ApJ*, 672, 83
 Martins, L. P., Rodríguez-Ardila, A., de Souza, R., et al., 2010, *MNRAS*, 406, 2168
 Merritt, D., & Ekers, R. D., 2002, *Science*, 297, 1310
 Merritt, D., 2006, *ApJ*, 648, 976
 Miller, J. S., Goodrich, R. W., & Mathews, W. G., 1991, *ApJ*, 378, 47
 Milosavljević, M., Merritt, D., Rest, A., et al., 2002, *MNRAS*, 331, L51
 Milosavljević, M., & Merritt, D., 2001, *ApJ*, 563, 34
 Minezaki, T., Yoshii, Y., Kobayashi, Y., et al., 2019, *ApJ*, 886, 150
 Modjaz, M., Moran, J. M., Kondratko, P. T., et al., 2005, *A&A*, 626, 104
 Müller Sánchez, F., Davies, R. I., Genzel, R., et al., 2009, *ApJ*, 691, 749
 Nixon, C. J., Cossins, P. J., & King, A. R., et al., 2011, *MNRAS*, 412, 1591
 Oknyansky, V. L., Winkler, H., Tsygankov, S. S., et al., 2019, *MNRAS*, 483, 558

Osterbrock, D. E., & Mathews, W. G., 1986, *ARA&A*, 24, 171
 Papaloizou, J. C. B., & Lin, D. N. C., 1984, *ApJ*, 285, 818
 Peters, P. C., 1964, *Phys. Rev.*, 136, 1224
 Peterson, B. M., 1993, *Pub. Ast. Soc. Pacific*, 105, 247
 Popović, L. Č., 2012, *New Astron. Rev.*, 56, 74
 Pringle, J. E., 1981, *ARA&A*, 19, 137
 Pringle, J. E., 1991, *MNRAS*, 248, 754
 Quach, D., Dyda, S., & Lovelace, R. V. E., 2015, *MNRAS*, 446, 622
 Raban, D. *et al.*, 2009, *A&A*, 394, 1325
 Rees, M. J., 1984, *ARA&A*, 22, 471
 Roedig, C., & Sesana, A., 2014, *MNRAS*, 439, 3476
 Runnoe, J. C., Eracleous, M., Pennell, A., *et al.*, 2017, *MNRAS*, 468, 1683
 Rybicki, G. B., & Lightman, A. P., *Radiation Processes in Astrophysics*, Wiley-Interscience Press (1979)
 Sanders, R. H., 1981, *Nature*, 294, 427
 Schawinski, K., *et al.*, 2015, *MNRAS*, 451, 2517
 Shakura, N. I., & Sunyaev, R., 1973, *A&A*, 24, 337
 Shi, J.-M., & Krolik, J. H., 2016, *ApJ*, 832, 22
 Songsheng, Y.-Y., Xiao, M., Wang, J.-M., *et al.*, 2020, *ApJ*, 247, 3
 Songsheng, Y.-Y., Wang, J.-M., & Li, Y.-R., 2019, *ApJ*, 883, 184
 Temi, P., Amblard, A., Gitti, M., *et al.*, 2018, *ApJ*, 858, 17
 Tremaine, S., *et al.*, 2002, *ApJ*, 574, 740
 Tremblay, G. R., Oonk, J. B. R., & Combes, F., *et al.*, 2016, *Nature*, 534, 218
 Valtonen, M. J., Lehto, H. J., Nilsson, K., *et al.*, 2008, *Nature*, 452, 851
 Vanden Berk, D. E., Richards, G. T., Bauer, A., *et al.*, 2001, *AJ*, 122, 549
 Volonteri, M., Madau, P., & Haardt, F., 2003, *ApJ*, 593, 661
 Wang, J.-M., Chen, Y.-M., & Zhang, F., 2006, *ApJ*, 647, L17
 Wang, J.-M., Hu, C., Li, Y.-R., *et al.*, 2009, *ApJ*, 697, L141
 Wang, J.-M., Songsheng, Y.-Y., Li, Y.-R., *et al.*, 2018, *ApJ*, 862, 171
 Wang, X.-W., & Yuan, Y.-F., 2012, *MNRAS*, 427, L1
 Winter, L. M., Mushotzky, R. F., Reynolds, C. S., *et al.*, 2009, *ApJ*, 690, 1322
 Yu, Q., 2002, *MNRAS*, 331, 935
 Zaino, A., Bianchi, S., Marinucci, A., *et al.*, 2020, *MNRAS*, 492, 3872

APPENDIX A: OBSERVATIONAL PROPERTIES

Polarized spectra. The polarized spectra of NGC 1068 show typical spectra of Seyfert 1 galaxies (Antonucci 1985; Miller *et al.* 1991) and hence demonstrate the existence of an obscured broad-line region (BLR) by a dusty torus. In light of the scenario, an orientation-based unification scheme was suggested for all Seyfert galaxies as well as for quasars (Antonucci 1993). Broad $H\beta$ line appears in the optical polarized spectra along with strong and broad Fe II emission lines. Using the polarized spectra, the black hole mass can be estimated by the virialized motion of BLR. We find the black hole mass of $(8.4 \pm 0.4) \times 10^6 M_\odot$ from the 5100 Å luminosity estimated from the [O III] line (Du *et al.* 2017), which is consistent with results estimated from 2–10 keV luminosity (Zaino *et al.* 2020).

It is important to note that the polarized $H\beta$ profile is asymmetric (Miller *et al.* 1991), implying complicated structures of the hidden BLR, at least existence of sub-structures of ionized gas (Du *et al.* 2018). Since the polarized lights to observers are from scatters of an electron screen vertically located at a distance of 100 pc from the galactic center, it will be very hard to observe variations of the polarized $H\beta$ line through a feasible length campaign. Actually, the Brackett γ line profiles are double-peaked, see Figure 4 in Martins *et al.* (2010). NGC 1068 is bright enough in near infrared for GRAVITY spectroastrometry to measure the differential phase curves. Signatures of CB-SMBHs could appear in the differential phase curves (Songsheng *et al.* 2019).

Dusty discs. The most important information for infrared continuum is the extinction, which can be estimated by near infrared

emission lines. The Brackett α broad line component observed by Infrared Space Observatory (ISO) constrains a lower limit of the extinction $A_{Br\alpha,4.05} \geq 2.4$, implying the extinction $A_K \geq 6$ in the K-band (Lutz *et al.* 2000). Observations of mid-infrared interferometric instrument (MIDI) for NGC 1068 reveal two spatially resolved regions: 1) inner and hot (> 800 K) zone with 1.35 pc long and 0.45 pc thick at a PA = -42° , and 2) outer and warm (~ 300 K) zone with 3×4 pc (Jaffe *et al.* 2004; Raban *et al.* 2009) but extended to 7 pc regions along the north-south axis (López-Gonzaga *et al.* 2014), and somehow may correspond to polar dust emission in the ionization cone. The gap between the NIR and MIR dust regions can be approximated by $R_* \approx 2.5$ pc, actually overlap with the velocity interface of the HCN gas map (Impellizzeri *et al.* 2019). We thus adopt it as the interface radius where the KHI is taking place.

GRAVITY onboard Very Large Telescope Interferometer (VLTI) observations find the dust sublimation radius $R_{\text{sub}} = 0.24$ pc, where hot dust particles (~ 1500 K) are responsible for NIR and MIR emissions with extinctions of foreground dust ($A_K = 5.5$) (Gravity *et al.* 2020). A structure with a hole has been found around 0.24 pc (Gravity *et al.* 2020). This radius agrees with the empirical relation established by NIR dust reverberation mapping of AGNs (Minezaki *et al.* 2019). However, the innermost part of the dusty disc is geometrically thin as $H/R \lesssim 0.1$, which is still much thicker than the Shakura-Sunyaev disc.

Maser disc. Water (and OH) masers observed by VLBI trace inner edge of the torus from a radius of 0.4 to ~ 1 pc with a PA = -45° completely different from radio jet (Greenhill *et al.* 1996, 1997; Gallimore *et al.* 1996b,c). The inclination of the maser disc is $\sim 80^\circ$ whereas an inclination of $\sim 70^\circ$ is obtained by fitting infrared continuum (Lopez-Rodriguez *et al.* 2018). Generally the maser disc aligns with the dusty disc though slightly orientated differently.

Radio morphology. A radio core source, called S_1 , associated with the disc of H_2O vapor megamaser emission has been found (Greenhill *et al.* 1996; Gallimore *et al.* 2001). It is interesting to find that S_1 overlaps with the inner prograde HCN disc (Impellizzeri *et al.* 2019). ALMA observations of 256 GHz continuum show very interesting features, not discussed in Ref (Impellizzeri *et al.* 2019), that the radio flux contours overlap with the velocity interface between the two counter rotating parts of the HCN disc, see Figure 2 in Ref (Impellizzeri *et al.* 2019).

APPENDIX B: CLOSE BINARY OF SUPERMASSIVE BLACK HOLES

As expected for several decades from the theory of the merger tree of galaxy evolution, CB-SMBHs (defined as those with separations less than 0.1 pc) evolved from dual galactic cores must be located in centers of some galaxies sometimes (Begelman *et al.* 1980; Volonteri *et al.* 2003). Most phenomenon of AGN activities can be explained by accretion onto a single SMBH (Rees 1984; Osterbrock & Mathews 1986), implying that most CB-SMBHs have finished the final mergers. Single epoch spectrum with double-peaked profiles cannot be used as a direct diagnostic of CB-SMBHs (Popovic 2012; Gaskell 2010). Though dual AGNs are quite common among galaxies (Comerford *et al.* 2013; Fu *et al.* 2015; Liu *et al.* 2018), however, observational evidence for CB-SMBHs is very elusive (Popovic 2012; Dotti *et al.* 2012). Though the radio map of NGC 7624 ($z = 0.0029$) shows two radio cores with a separation of 0.35 pc in the nucleus and plausibly implies a candidate binary black holes (Kharb *et al.* 2017), none of CB-SMBHs are identified so

far. A very brief summary is given below about the progress of searching for CB-SMBHs.

The final parsec problem. The formation of massive black hole binaries is unavoidable as a outcome of successive mergers of galaxies, however, it turns out that the decay of the binary orbits in a real galaxy would be expected to stall at separations of parsec scales unless some additional mechanism is able to efficiently remove the orbital AM (Milosavljević & Merritt 2001). At large separations, dynamical friction of the binaries with background stars controls orbital evolution (Milosavljević & Merritt 2001; Yu 2002; Wang & Yuan 2012), but becomes inefficient when the mass enclosed in the orbits are comparable in gas-poor environment and hardly evolve into stages of radiating gravitational waves. This is the so-called “final parsec problem” (Begelman et al. 1980; Milosavljević & Merritt 2001).

Numerous simulations show that the gas-rich environment can efficiently absorb and transfer the orbital AM through the tidal interaction with the prograde CBD (Escala et al. 2005; MacFadyen & Milosavljević 2008; Cuadra et al. 2009; Lodato et al. 2009), or the retrograde (Nixon et al. 2011; Roedig & Sesana 2014; Bankert et al. 2015). However, the real situations are complicated by successive random accretion of clumpy clouds formed in circumnuclear regions (Tremblay et al. 2016; Temi et al. 2018), which have been found as an efficient clue to harden binary black holes from simulations (Goicovic et al. 2017, 2018). Fortunately, such a configuration of accretion onto binary black holes has been found in NGC 1068 by ALMA (Impellizzeri et al. 2019), which provides unique opportunity to investigate the orbital evolution predicted by simulations.

Signatures of CB-SMBHs. The suggested signatures so far are: 1) periodicity of long term radio or optical variations of AGNs from a few years to a few tens of years, which is regarded as results of modulation of the orbital motion of CB-SMBHs; 2) ultraviolet deficit of continuum rising from the central cavity of the CBD governed by the tidal torques of the binary; 3) shifts of red and blue peaks of broad emission lines in long term variations similar to normal binary stars; 4) deficit profile of brightness of galactic centers as a result of ejection of stars through interaction of stars with the binary black holes; 5) 2-dimensional kinematic maps of broad emission lines in AGNs showing signatures of two point potentials generated through reverberation mapping campaigns; 6) GRAVITY (or Extremely Large Telescope: ELT) with spectroastrometry may reveal some signals of double BLRs. Additionally, X-shaped radio jet was regarded as a signature of CB-SMBHs (Merritt & Ekers 2002), but it hardly applies to measure orbital parameters of the binaries.

Great efforts have been made to search for periodicity of AGN long-term variations over several decades. Nowadays, a sample composed of about 100 AGNs was built up through Catalina Real-time Transient (Graham et al. 2015a), among which PG 1302-102 is the best one with a period of 5 yrs (Graham et al. 2015b; D’Orazio et al. 2015). Other three objects with periodical variations are OJ 287 in radio (Valtonen et al. 2008), NGC 5548 with a period of about ~ 13 yrs over 40 yrs (Li et al. 2016), and Akn 120 with a period of ~ 20 yrs over the last 40 yrs (Li et al. 2019). Progress in this way is quite slow so far unless the future LSST can efficiently discover some AGNs with short periods from the fast large scale of time domain surveys.

Continuum features of CB-SMBHs radiated from accretion result from the cavity of the CBD governed by tidal interaction (Gültekin & Miller 2012). However, the shapes of UV continuum are easily affected by dust extinctions (Leighly et al. 2016), making that it is hardly useful to justify candidates of CB-SMBHs in practice.

Moreover, it has been shown that the binary black holes are peeling off gas from the inner edge of the CBD making the accretion rates quite high (the rates still comparable with the accretion rates of the CBD) (Farris et al. 2014; Shi & Krolik 2016; Bowen et al. 2019). For the current case of NGC 1068, the binary black holes are peeling off gas for accretion to radiate gravitational energies.

Searching for systematically periodical shifts of AGNs with double-peaked profiles is expected to find CB-SMBHs (Runnoe et al. 2017; Doan et al. 2020). Similar to classical binary stars, the double BLRs orbiting around the mass center of the binary black holes will lead to opposite shifts of the red and blue peaks with orbital phases. The long term campaigns are expected to carry out in next a few years, but SDSS J0938+0057, SDSS J0950+5128, and SDSS J1619+5011 in this sample showed systematic and monotonic velocity changes consistent with the binary hypothesis (Runnoe et al. 2017).

As a consequence of interaction with CB-SMBHs, as shown by numerical simulations (Ebisuzaki et al. 1991; Milosavljević et al. 2002; Merritt 2006), stars are ejected from galactic center, forming a “mass deficit” in its central part. Actually, it does not appear to have a pronounced and unambiguously detectable effects on the density profile. Even though it works for searching for CB-SMBHs, on the other hand, this method doesn’t apply to determine orbital parameters to test properties of gravitational waves, and the same shortcomings for the identifications of AGNs with X-shaped jet morphology.

Reverberation mapping of AGNs is a powerful tool to probe the kinematics and structure of the BLR (Peterson 1993). Usually, BLRs have relatively stable structures justified from the large sample of SDSS quasars (Vanden Berk et al. 2001) though they are variable on timescale of years. In principle, the broad-line gas is governed by the central black hole potential, and therefore it is expected to show signatures of CB-SMBH orbital motion from the 2-dimensional velocity delay map from reverberation mapping of AGNs (Wang et al. 2018; Songsheng et al. 2020; Kovacović et al. 2020). This reasoning also depends on the orbital motion, but the advantage of this scheme is obvious that the campaigns can be performed in seasons and does not require long-term monitoring as the approach of period searching. A campaign called as Monitoring AGNs with H β Asymmetry (MAHA) has been conducted with Wyoming Infrared Observatory (WIRO) Telescope targeting on objects with various H β profiles (Du et al. 2018). Results are expected to be carried out shortly.

GRAVITY/VLTI provides the highest spatial resolution in NIR. The differential phase curves measured by GRAVITY depends on the geometric structures and kinematics of ionized gas emitting broad lines. For CB-SMBHs, there are several simplest configurations of AM distributions of individual BLRs and binary orbital motion. Details of the phase curves have been explored for signals of CB-SMBHs (Songsheng et al. 2019). We are expecting to jointly observe some Seyfert 2 galaxies through ALMA and GRAVITY, which can be selected by checking optical polarized spectra with complicated profiles. We hope discover more Seyfert 2 galaxies with the CRDs like in NGC 1068.

Some AGNs show that rotation curves of masers don’t follow the Keplerian law. The radial self-gravity of the maser disc could be important (Hure et al. 2011), however, infrared emissions doesn’t support this hypothesis. Moreover, ALMA measurements of molecular gas mass in NGC 1068 is significantly smaller than the black hole. It is a curiosity that the maser disc shares different dynamics from the molecular gas if inspecting details (Greenhill et al. 1997; Impellizzeri et al. 2019). On the other hand, it could be plausible, if

speculate, that CB-SMBHs work in these objects. Detailed dynamical modeling of the maser or molecular gas at parsec scales will allow us to determine some of orbital parameters, which are keys to test properties of nano-Hz gravitational waves.

APPENDIX C: CAVITY OF THE CBD

Dynamics of gas at parsec scales revealed by the water megamaser (Greenhill et al. 1996; Gallimore et al. 1996a) and HCN/HCO⁺ ($J = 3 - 2$) molecular gas (Imanishi et al. 2018; Impellizzeri et al. 2019; García-Burillo et al. 2019) provides strong constraints on the accretion disc size of the central black hole and hence spatial distribution of gas in the compact regions. For NGC 1068, the black hole mass is of $M_{\bullet} = (0.8 - 1.7) \times 10^7 M_{\odot}$ and the bolometric luminosity is $L_{\text{Bol}} \approx 2.0 \times 10^{45} \text{ ergs s}^{-1}$ from multiwavelength data (Gravity et al. 2020), we thus have the Eddington ratio of $\lambda_{\text{Edd}} \approx 1$, implying that NGC 1068 has high accretion rates. The strong Fe II emissions in the polarized optical spectra (Miller et al. 1991) shows the key feature of high rates (Du & Wang 2019).

Recent ALMA observations of HCN/HCO⁺ ($J = 3 - 2$) emission lines (Impellizzeri et al. 2019; García-Burillo et al. 2019) show that the extrapolation of the rotation curve of the 0.5 – 1.2 pc HCN molecular gas, which agrees with that of the water maser (Greenhill et al. 1996; Gallimore et al. 1996b), is consistent with the rotation curve extended to 7 pc disc (Impellizzeri et al. 2019). This indicates that the enclosure mass is still dominated by the central black hole at a few parsec scales (Hure et al. 2002). With help of the gas disc mass (M_{AD}) estimated from Equation (D2), we have upper limit of its outer boundary of $R_{M_{\bullet}} \leq 1.95 \times 10^5 (\alpha_{0.1} M_7)^{16/25} \dot{m}_{10}^{-14/25} R_{\text{Sch}} \approx 0.19 \text{ pc}$ from $M_{\text{AD}}(\leq R) \leq M_{\bullet}$. With the gas dynamics, we draw a conclusion that the disc must be truncated at least $R_{M_{\bullet}}$. Indeed, the HCN molecular gas is $M_{\text{gas}}^{\oplus} \sim 9 \times 10^5 M_{\odot}$ ($\lesssim 3 \text{ pc}$: corresponding to a surface density $\Sigma_{\text{gas}}^{\oplus} \approx 3 \times 10^4 M_{\odot} \text{ pc}^{-2}$ and a number density of $n_{\oplus} \approx 2.2 \times 10^6 \text{ cm}^{-3}$) measured by ALMA (Imanishi et al. 2018; García-Burillo et al. 2019), which is smaller than M_{\bullet} . At this edge of the disc, its temperature is $T_{\text{eff}}(R_{M_{\bullet}}) \approx 120 (\dot{m}_{10}/M_7)^{1/4} (R/R_{M_{\bullet}})^{-3/4} \text{ K}$ much lower than the dust sublimation temperature, and the disc surface density is $\Sigma_{\text{AD}} \approx 5.7 \times 10^7 M_{\odot} \text{ pc}^{-2}$. There is another critical radius corresponding to the dust sublimation temperature, we have $R_{\text{dust}} = 0.04 (\dot{m}_{10}/M_7)^{1/3} R_{M_{\bullet}}$. According to the Kennicutt-Schmidt law (Kennicutt 1998), this high surface density of gas between $(R_{\text{dust}}, R_{M_{\bullet}})$ with low temperatures are undergoing starbursts with a rate of $\dot{R} \approx 4.8 M_{\odot} \text{ yr}^{-1}$, resulting in an infrared luminosity of $L_{\text{MIR}}^* \approx 1.1 \times 10^{44} \text{ ergs s}^{-1}$ radiating between 8-100 μm . Such a bright mid- and far infrared emission doesn't appear in the spectral energy distributions (the observed MIR luminosity is $L_{\text{MIR}}^{\text{obs}} \lesssim 1.0 \times 10^{43} \text{ ergs s}^{-1}$ estimated from Figure 5 in Ref (Gravity et al. 2020)). Considering the constraints of $L_{\text{MIR}}^* < L_{\text{MIR}}^{\text{obs}}$, we have the outer boundary radius $R_{\text{AD}} \lesssim \left(L_{\text{MIR}}^{\text{obs}} / L_{\text{MIR}}^* \right) R_{M_{\bullet}} \lesssim 0.1 R_{M_{\bullet}} = 0.019 \text{ pc}$, which is consistent with R_{dust} . This means that the $R_{\text{AD}} - R_{M_{\bullet}}$ region should be a cavity of gas (or a low-density region though we are not able to estimate its density currently). On the other hand, GRAVITY (Gravity et al. 2020) measured the radius of the dust sublimation $R_{\text{sub}} \approx 0.24 \pm 0.03 \text{ pc}$ and discovered an extended structure with a central hole with the radius of R_{sub} by imaging the central regions of NGC 1068 at 2 μm , agreeing with $R_{M_{\bullet}} \lesssim R_{\text{sub}}$. All these provide evidence for that the 2 μm -imaged hole is a central cavity of gas.

Such a cavity is a natural consequence of tidal interaction of the

circumnuclear disc (CND) with the binary black holes (Artymowicz et al. 1994; Escala et al. 2005; MacFadyen & Milosavljević 2008; Cuadra et al. 2009; Lodato et al. 2009) if they exit subsequently evidenced by the CRD in the galactic center of NGC 1068. According to analytical analysis, the inner radius of the CND, which is denoted the circumbinary disc (CBD), should be around $R_{\text{CBD}} \approx R_{\text{sub}} = 2A$, where A is the separations of the binary black holes. From the 2 μm -imaged hole, we have $A \approx 0.12 \text{ pc}$.

APPENDIX D: ACCRETION DISCS

Given the black hole mass of $M_{\bullet} = 10^7 M_{\odot}$ in NGC 1068, distance scales are: $0.1 \text{ pc} \approx 114 \text{ lt d} \approx 10^5 R_{\text{Sch}}$. The dimensionless accretion rate is defined as $\dot{m} = \dot{M}/\dot{M}_{\text{Edd}} c^{-2} = 10 \eta_{0.1}^{-1} \lambda_{\text{Edd}}$ from $L_{\text{Bol}} = \eta \dot{M} c^2$, where $\eta_{0.1} = \eta/0.1$ is the radiative efficiency, L_{Edd} is the Eddington luminosity, $\lambda_{\text{Edd}} = L_{\text{Bol}}/L_{\text{Edd}}$ is the Eddington ratio and \dot{M} is the accretion rates. In the outer part of the Shakura-Sunyaev disc (Shakura & Sunyaev 1973), where gas pressure dominates over radiation pressure and absorption over Thompson scattering, the surface density is given by

$$\Sigma_{\text{d}} = 1.88 \times 10^7 \alpha_{0.1}^{-4/5} M_7^{1/5} \dot{m}^{7/10} r_5^{-3/4} M_{\odot} \text{ pc}^{-2}, \quad (\text{D1})$$

and the total mass of the accretion disc within R ,

$$M_{\text{AD}}(\leq R) \approx 8.67 \times 10^5 \alpha_{0.1}^{-4/5} M_7^{1/5} \dot{m}^{7/10} r_5^{5/4} M_{\odot}. \quad (\text{D2})$$

In light of the Toomre's parameter, the accretion disc becomes vertically self-gravitating at a radius of $R_{\text{SG}}/R_{\text{Sch}} \approx 500 \alpha_{0.1}^{2/9} M_7^{-2/9} \dot{m}^{4/9}$ (Laor & Netzer 1989). However, we are interested in the constraints on the AD size due to radial self-gravitating effects in this paper. Viscosity dissipates gravitational energy leading to effective temperature of disc surfaces

$$T_{\text{eff}} = \left(\frac{3}{8\pi} \frac{GM_{\bullet} \dot{M}}{\sigma_{\text{SB}} R^3} \right)^{1/4} = 111.0 M_7^{-1/4} \dot{m}^{1/4} r_5^{-3/4} \text{ K}, \quad (\text{D3})$$

where σ_{SB} are the Stefan-Boltzmann constant, respectively.